New Journal of Physics
The open-access journal for physics

Elastic waves in phononic monolayer granular membranes

Vincent Tournat[1,4], Isabel Pèrez-Arjona[2], Aurélien Merkel[1], Victor Sanchez-Morcillo[2] and Vitalyi Gusev[3]

[1] LAUM, CNRS, Université du Maine, Av. O Messiaen, 72085 Le Mans, France
[2] IGIC, Universidad Politècnica de Valencia, Crta. Natzaret-Oliva s/n, 46730 Grau de Gandia, Spain
[3] LPEC, CNRS, Université du Maine, Av. O Messiaen, 72085 Le Mans, France
E-mail: vincent.tournat@univ-lemans.fr

New Journal of Physics **13** (2011) 073042 (15pp)
Received 6 April 2011
Published 29 July 2011
Online at http://www.njp.org/
doi:10.1088/1367-2630/13/7/073042

Abstract. The vibrational properties of out-of-plane elastic waves in hexagonal monolayer granular membranes were studied theoretically. The predicted propagation modes involve an out-of-plane displacement and two rotations with axes in the membrane plane. Shear and bending rigidities at the contact between beads were considered. Both the cases of freely suspended membranes and membranes coupled to a rigid substrate were analyzed. Dispersion relations and the existence of band gaps are presented and discussed for various contact properties. For freely suspended membranes with sufficient contact bending rigidity, it is shown that complete band gaps exist. The results obtained may be of interest for testing with acoustic waves the elasticity of recently developed granular membranes composed of nanoparticles (of interest because of their phoxonic properties) and more generally for the control of designing devices for membrane wave propagation.

[4] Author to whom any correspondence should be addressed.

Contents

1. Introduction

The study of the properties of phononic crystals and of the control of elastic/acoustic wave propagation by metamaterials has become a very active area of research, owing to their numerous interesting applications in, for example, high-frequency surface acoustic wave filtering [1, 2]. There is also much interest among researchers in the study of acoustic metamaterials, related to new or enhanced wave processes including, for example, acoustic cloaking, negative refraction or subwavelength imaging [3–6]. Although devices involving plates or membranes have been widely used, most of the recent studies on metamaterials concern three-dimensional (3D) materials supporting bulk or surface acoustic waves [2], whereas very little has been reported on plate or membrane waves [7–9]. Recently, even at the smallest scale suitable for gigahertz acoustic applications, nanogranular media were produced, allowing simultaneously both photonic and phononic (phoxonic) functionalities [10]. For instance, technologies have been developed for building crystals consisting of nanoparticles [11–15], ordered monolayers of particles [16–18] and freely suspended membranes composed of a single layer of periodically ordered particles [19–21].

To describe the high-frequency (short-wavelength) vibrational behavior of such periodic structures composed of interacting discrete particles, the continuous approximation of the elasticity theory becomes inadequate and the discrete nature of the medium should be explicitly taken into account [22, 23]. For most of the discrete structures, including atomic crystals, the particles can be considered as point masses interacting through central forces [22]. However, to model the elastic behavior of granular crystals composed of finite-size particles interacting through forces located at the contact points between particles [24–27], it becomes necessary to take into account the particle dimensions, the finite rotational inertia (rotational degrees of freedom) and the interactions through non-central forces. In particular, in addition to shear and longitudinal acoustic modes, rotational (micro-rotational) modes are predicted in such structures [28, 29].

For more than a century, there exist theories for the description of long-wavelength acoustic wave propagation in the so-called micropolar media, the Cosserat continuum theory (micropolar elasticity) [30–32]. However, when wavelength is shortened and becomes comparable to the particle size, these theories are unable to describe the dispersive phononic properties. Nevertheless, the predictions of the Cosserat continuum theory (micropolar elasticity) [30–32], which incorporates in continuous elasticity the possible rotations of micro-mechanical elements

composing micro-inhomogeneous materials such as microcrystalline materials, can be used for a comparison to the low frequency limit of the theories for elastic wave propagation in ordered granular structures. This comparison provides an opportunity to identify micro-mechanical interactions contributing to particular elastic constants appearing in Cosserat-type theories of micro-inhomogeneous but macroscopically homogeneous and isotropic materials in addition to two constants of classical linear elasticity of micro-homogeneous isotropic materials [33–35].

It should be mentioned that, although a general theoretical approach for analysis of acoustic waves in discrete periodic systems has been presented earlier [36], the analysis of 2D–3D structures composed of finite size particles has been limited mostly to predictions of the properties of bulk longitudinal and shear acoustic-type elastic modes [37–40] and guided shear acoustic modes in macroscopically inhomogeneous granular crystals [41–43]. Only in recent years the rotational, coupled rotational/transversal and transversal/rotational modes have been included in analyses [44–46]. The analysis of 2D structures, which includes rotational degrees of freedom in particle motion, has been reported only for in-plane motion [33–35]. Out-of-plane motion has been analyzed only for surface acoustic waves on discrete structures of point masses [23] and in the framework of the Cosserat continuum models [47, 48].

Here, we present the results of a theoretical investigation of the elastic modes in freely suspended granular membranes and in membranes interacting with a substrate. The out-of-plane motion incorporating rotations of particles is analyzed for the first time. The developed theory provides the basis for the application of elastic waves in the non-destructive evaluation and testing of granular membranes and in the testing of the adhesion of a particle monolayer to a substrate.

2. Model

We consider an infinite monolayer membrane composed of periodically ordered spherical particles, arranged in a hexagonal lattice (figure 1(a)). The structure is supposed to consist of homogeneous spheres with radius R and is characterized by a lattice constant $a = 2R$. The corresponding first Brillouin zone is shown in figure 1(b), and the modulus of the reciprocal vector k is $4\pi/(\sqrt{3}a)$.

2.1. Shear rigidity of the contacts

In order to analyze the out-of-plane modes of the membrane, we model the shear forces at the contacts as springs, characterized by a constant shear rigidity ξ at the contact. The elongation of the springs introduces forces and momenta that induce the motion of the particles: out-of-plane displacement ($\boldsymbol{u}$) and in-plane rotation angles φ and ψ (φ-rotation with the axis in the x-direction and ψ-rotation with the axis in the y-direction; figure 1(b)).

We present the equations of motion for the central particle, which are given by the equation for the displacement u_0 of the center of the central particle, and the equations for the rotations φ_0 and ψ_0:

$$m\ddot{u}_0 = -\xi\left[(\delta u_1 + \delta u_4) + (\delta u_3 + \delta u_6) + (\delta u_2 + \delta u_5)\right], \tag{1}$$

$$I\ddot{\varphi}_0 = \frac{\sqrt{3}}{2}\xi R\left[(\delta u_1 - \delta u_4) - (\delta u_3 - \delta u_6)\right], \tag{2}$$

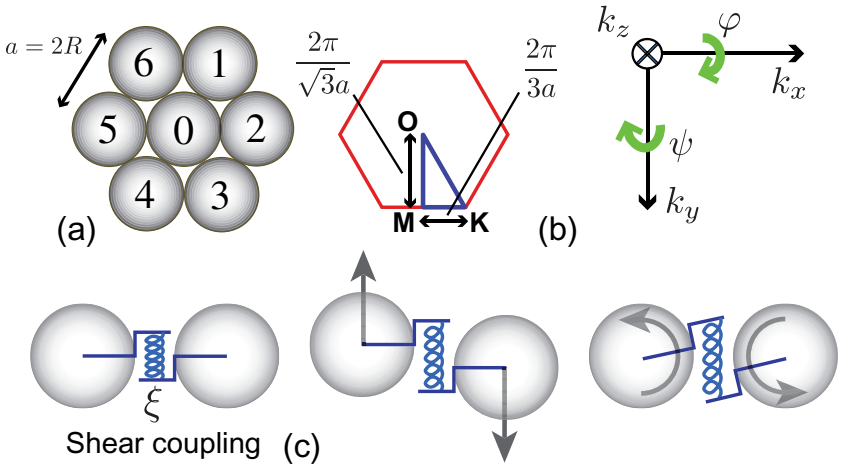

Figure 1. (a) Geometrical arrangement of the beads in the elementary cell of the hexagonal membrane crystal. (b) Definitions of the Brillouin zone and coordinate axes. (c) Activation of shear rigidity by particle displacements and rotations.

$$I\ddot{\psi}_0 = \frac{R}{2}\xi\left[(\delta u_1 - \delta u_4) + (\delta u_3 - \delta u_6)\right] + R\xi\left[\delta u_2 - \delta u_5\right], \tag{3}$$

where m is the mass of the particle and, for the particular case of homogeneous spheres, the momentum of inertia is $I = \frac{2}{5}mR^2$. The term δu_i denotes the elongation of the spring at the contact between the central and i-particle, i.e. the relative displacement between 0 and i-particle at the contact point. The form of relative displacements δu_i can be given in terms of particle displacements in the z-direction and rotations. For the six particles surrounding the central one in a cell of the lattice, relative displacements are explicitly given by the expressions

$$\delta u_1 = u_{0/1} - u_{1/1} = u_0 - u_1 - \frac{\sqrt{3}}{2}R\left(\varphi_0 + \varphi_1\right) - \frac{1}{2}R\left(\psi_0 + \psi_1\right), \tag{4}$$

$$\delta u_4 = u_{0/4} - u_{4/4} = u_0 - u_4 + \frac{\sqrt{3}}{2}R\left(\varphi_0 + \varphi_4\right) + \frac{1}{2}R\left(\psi_0 + \psi_4\right), \tag{5}$$

$$\delta u_3 = u_{0/3} - u_{3/3} = u_0 - u_3 + \frac{\sqrt{3}}{2}R\left(\varphi_0 + \varphi_3\right) - \frac{1}{2}R\left(\psi_0 + \psi_3\right), \tag{6}$$

$$\delta u_6 = u_{0/6} - u_{6/6} = u_0 - u_6 - \frac{\sqrt{3}}{2}R\left(\varphi_0 + \varphi_6\right) + \frac{1}{2}R\left(\psi_0 + \psi_6\right), \tag{7}$$

$$\delta u_2 = u_{0/2} - u_{2/2} = u_0 - u_2 - R\left(\psi_0 + \psi_2\right), \tag{8}$$

$$\delta u_5 = u_{0/5} - u_{5/5} = u_0 - u_5 + R\left(\psi_0 + \psi_2\right), \tag{9}$$

where the expressions for the displacements of particle i in the contact point with particle j ($u_{i/j}$) are given in the appendix, and φ_i and ψ_i are the rotations of the i particle with the axes collinear to the x- and y-directions, respectively.

The motion equations can be written for the new variables $\Phi = R\varphi$ and $\Psi = R\psi$ (the arcs on the particle surface) and solved in the form of plane waves

$$\vec{v} = \begin{pmatrix} u(x,y,t) \\ \Phi(x,y,t) \\ \Psi(x,y,t) \end{pmatrix} = \begin{pmatrix} u \\ \Phi \\ \Psi \end{pmatrix} e^{i\omega t - ik_x x - ik_y y} \tag{10}$$
$$= \begin{pmatrix} u \\ \Phi \\ \Psi \end{pmatrix} e^{i\omega t - ik_x x_0 - ik_y y_0} e^{-ik_x \Delta x - ik_y \Delta y},$$

where (x_0, y_0) are the coordinates of the central particle. We note that only the relative coordinates $(\Delta x, \Delta y)$ between the central particle and the neighbor particles are involved in the out-of-plane modes of the membrane.

After the substitution of equations (4)–(9) into the system of equations of motion (1)–(3) and plane-wave substitution with the help of equation (10), the equation of motion can be written in the form

$$\mathbf{S}\vec{v} = 0. \tag{11}$$

Normalizing the distances to the lattice constant a, the elements of the matrix $\mathbf{S}$ are then given by

$$S_{11} = \Omega^2 - \sin^2(\alpha-\beta) - \sin^2(\alpha+\beta) - \sin^2(2\alpha), \tag{12}$$

$$S_{12} = -i\frac{\sqrt{3}}{4}\{\sin[2(\alpha+\beta)] - \sin[2(\alpha-\beta)]\}, \tag{13}$$

$$S_{13} = \frac{i}{4}\{\sin[2(\alpha-\beta)] + \sin[2(\alpha+\beta)] + 2\sin(4\alpha)\}, \tag{14}$$

$$S_{21} = i\frac{\sqrt{3}}{4}\{\sin[2(\alpha+\beta)] - \sin[2(\alpha-\beta)]\}, \tag{15}$$

$$S_{22} = \frac{2}{5}\Omega^2 - \frac{3}{4}\left[\cos^2(\alpha-\beta) + \cos^2(\alpha+\beta)\right], \tag{16}$$

$$S_{23} = \frac{\sqrt{3}}{4}\left[\cos^2(\alpha+\beta) - \cos^2(\alpha-\beta)\right], \tag{17}$$

$$S_{31} = -\frac{i}{4}\{\sin[2(\alpha+\beta)] + \sin[2(\alpha-\beta)] + 2\sin(4\alpha)\}, \tag{18}$$

$$S_{32} = \frac{\sqrt{3}}{4}\left[\cos^2(\alpha+\beta) - \cos^2(\alpha-\beta)\right], \tag{19}$$

$$S_{33} = \frac{2}{5}\Omega^2 - \frac{1}{4}\left[\cos^2(\alpha-\beta) + 4\cos^2(2\alpha) + \cos^2(\alpha+\beta)\right], \tag{20}$$

where we have defined $\Omega^2 = \omega^2/(4\omega_0^2)$ with $\omega_0^2 = \xi/m$ and $\alpha = \frac{1}{4}k_x a$, $\beta = \frac{\sqrt{3}}{4}k_y a$.

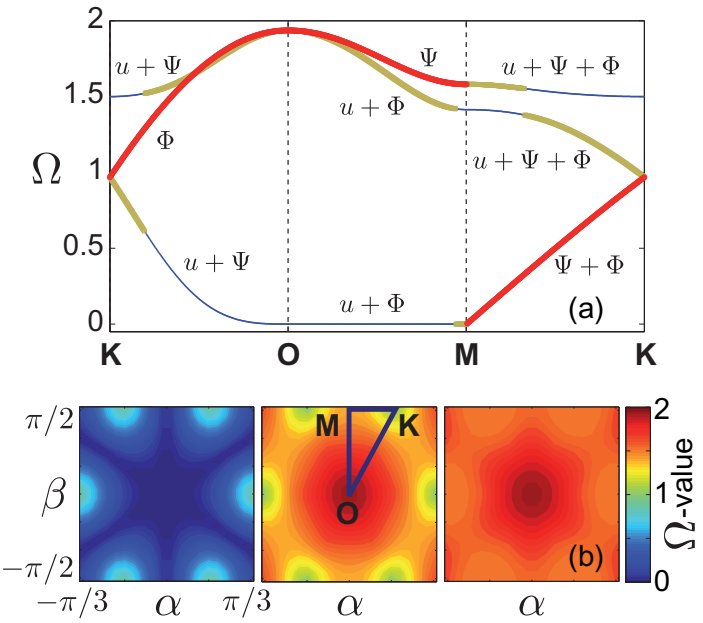

Figure 2. (a) Dispersion curves along the path (KOMK) in the case where only shear forces between beads are taken into account. Red curves correspond to pure rotation modes, blue curves to coupled displacement–rotation modes (with predominance of displacement) and yellow curves to couple displacement–rotation modes (with predominance of rotation). (b) Iso-surface plots of Ω for the lowest eigenvalue (left), the middle eigenvalue (center) and the highest eigenvalue (right), obtained for each couple (α, β).

The Ω–k dispersion curves shown in figure 2(a) are obtained from $\det(\mathbf{S}) = 0$. The dispersion curves are depicted, following the KOMK path in the first Brillouin zone [2], in figure 1(b). In the new normalization ($a = 1$) these points correspond, in the reciprocal space, to $\mathrm{O} \equiv (0, 0)$, $\mathrm{M} \equiv (0, \pi/2)$ and $\mathrm{K} \equiv (\pi/6, \pi/2)$. The segments OM and OK correspond to waves propagating along symmetry directions. The segment OM corresponds to the y-direction. Due to the symmetry of the structure, any rotation of the propagation direction of $n\pi/3$ (with n being an integer) relative to the z-axis provides no modification of the propagation properties. Accordingly, the segment OK is a propagation direction equivalent to the x-direction, i.e. it exhibits the same propagation properties. In figure 2(a), different propagation directions are separated by dashed lines and the nature of the modes is labeled. The plotted eigenvalues have been colored relatively to the eigenvectors that have been classified. Red curves correspond to pure rotation modes, blue curves to coupled displacement–rotation modes (with a predominance of displacement) and yellow curves to coupled displacement–rotation modes (with a predominance of rotation). The eigenmodes of the infinite membrane motion are consisting, in general, of three different components (the out-of-plane displacement u and two in-plane rotation angles Φ and Ψ). Nevertheless, for particular propagation directions one of the components is decoupled from the others. In the case of a propagative wave in the k_x (respectively k_y) direction, a mode called Φ-mode (respectively Ψ-mode) and shown in red in figure 2 appears uncoupled from the mixed modes $(u + \Psi)$ (respectively $(u + \Phi)$). In the case of waves propagating along the y-direction $(0 < \beta < \pi/2)$, we note a zero-frequency

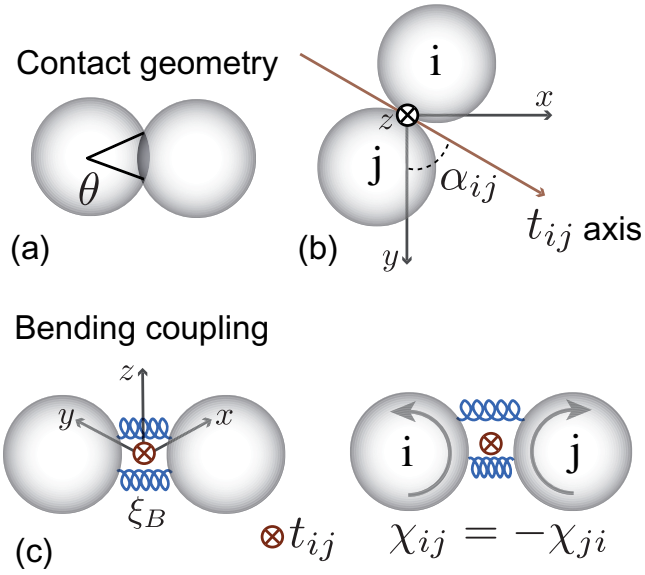

Figure 3. Schematic diagram of the contacts with bending rigidity and definition of the angles and axes.

$(u+\Phi)$-mode, whereas two other modes corresponding to $u+\Phi$ and Ψ-modes propagate with frequencies $\Omega^2 = \frac{15}{4}(1 - \frac{7}{15}\sin^2\beta)$ and $\Omega^2 = \frac{15}{4}(1 - \frac{1}{3}\sin^2\beta)$, respectively. For the x-direction, a compact presentation of the dispersion relation can be obtained for the uncoupled Φ-mode: $\Omega^2 = \frac{15}{4}(1 - \sin^2\alpha)$, where $0 < \alpha \leqslant \pi/3$. For the particular plane vibrations with $k_x = 0$, $k_y = 0$, the three components are decoupled from each other: the two modes corresponding to rotations have the same eigenfrequency given by $\Omega^2 = 15/4$, whereas the displacement mode has zero frequency.

The frequencies Ω satisfying $\det(\mathbf{S}) = 0$ for any propagation direction in the plane (α, β) are shown in figure 2(b). For the three obtained eigenvalues of $\mathbf{S}$, the sixth-order symmetry around the z-axis is observed on these iso-surface plots.

The zero frequency $u+\Phi$-mode (non-propagative mode of zero group velocity) exists because there are such combinations of displacements and rotations of the particles which do not lead to the loading of the contact (to the elongation of the shear spring). In other words, in the model presented above, there are configurations of the displaced and rotated particles which have the same energy as the background configuration with zero displacement and zero rotation. The analysis demonstrates that the zero mode is allowed, particularly because in the model developed above (figure 1(c)), the rotations of two neighboring particles with the same angle but opposite directions do not cause any loading of the contact. In reality, it is the bending rigidity of the contacts that counteracts this type of motion (figure 3(c)). Whereas the bending rigidity plays a negligible role in comparison with shear rigidity in unconsolidated granular crystals [44–46], it plays an important role when the contacts are consolidated (sintered).

2.2. *Bending rigidity of the contacts*

We model, in the following, the bending rigidity of sintered contacts of radius $r \simeq R\theta \ll R$ by including in the contact description (additionally to the shear spring) two springs with normal

rigidities ξ_B (see figure 3(c)). They are oriented in the membrane plane and located at the lowest and highest points of the contact along the z-direction.

In this extremely simplified presentation of the physical nature of bending rigidity, even rotations of the neighboring particles in opposite directions but with the same angle will cause elongation of one of the springs and contraction of the other. The corresponding forces have non-zero momenta relative to the rotation axes and will try to make the particles return to their equilibrium state. For example, an additional (bending-related) momentum of forces acting on particle 0 because of the rotations of particles 0 and 2 relative to the y-axis can be described by

$$M_{02}^{\Psi} = -\frac{r^2}{2}\xi_B(\Psi_0 - \Psi_2). \tag{21}$$

In the proposed simple model, bending-related momenta are effective not only for contacts located on the rotation axis (e.g. for the contact between particles 0 and 2 in the case of their rotation along the x-axis). In the latter case, spin (torsional) rigidity of the contact [49] could play a role.

As a consequence of the contact bending rigidity, which is a function of both ξ_B and the dimension $R\theta$ of the contact along the z-axis (where θ is the contact angular dimension; see figure 3(a)), there is a moment along the t_{ij}-axis tangent to the contact between neighbor beads i and j in the x–y-plane. This moment exists even if the beads rotate relative to the direction t_{ij} to exactly opposite angles $\chi_{ij} = -\chi_{ji}$ (figure 3(c)).

Here, the angle χ_{ij} of rotation of the bead i relative to the axis t_{ij} is equal to

$$\chi_{ij} = \varphi_i \sin\alpha_{ij} + \psi_i \cos\alpha_{ij}, \tag{22}$$

where $\alpha_{ij} = \alpha_{ji}$ is the angle between the t_{ij}-axis and the y-axis ($\alpha_{01} = \alpha_{04} = \pi/3$, $\alpha_{03} = \alpha_{06} = 2\pi/3$, $\alpha_{02} = \alpha_{05} = 0$).

Due to bending rigidity, the sum of the bending momenta provides the following contributions to the momenta rotating the central beads ($j = 0$) along the x- and y-axes:

$$M_\varphi = \frac{\theta^2}{2}\xi_B R^2\left[(\chi_{10} - \chi_{01} - \chi_{04} + \chi_{40})\sin(\pi/3) + (\chi_{30} - \chi_{03} - \chi_{06} + \chi_{60})\sin(\pi/3)\right], \tag{23}$$

$$\begin{aligned} M_\psi = \frac{\theta^2}{2}\xi_B R^2[&(\chi_{10} - \chi_{01} - \chi_{04} + \chi_{40})\cos(\pi/3) + (\chi_{30} - \chi_{03} - \chi_{06} + \chi_{60})\cos(2\pi/3) \\ &+ (\chi_{20} - \chi_{02} - \chi_{05} + \chi_{50})]. \end{aligned} \tag{24}$$

The matrix S is modified in the following additional terms:

$$\Delta S_{22} = -\frac{3}{4}p_B\left[\sin^2(\alpha+\beta) + \sin^2(\alpha-\beta)\right], \tag{25}$$

$$\begin{aligned} \Delta S_{23} &= \Delta S_{32} \\ &= -\frac{\sqrt{3}}{4}p_B\left[\sin^2(\alpha-\beta) - \sin^2(\alpha+\beta)\right], \end{aligned} \tag{26}$$

$$\Delta S_{33} = -p_B\left\{\left[\sin^2(\alpha+\beta) + \sin^2(\alpha-\beta)\right]/4 + \sin^2(2\alpha)\right\}, \tag{27}$$

where the non-dimensional bending parameter p_B has been defined as $p_B = \frac{\theta^2}{2}\frac{\xi_B}{\xi}$. By considering bending rigidity of the contact, the rotation around the x-axis influences the rotation

around the y-axis and vice versa. The dispersion relations of the membrane are modified by the presence of bending rigidity, as can be noted in the modes corresponding to the propagation along the y-axis (OM segment), where a second coupled mode propagates even for small values of the bending parameter (figure 4).

The frequencies of all the modes in the points M, K and O can be found analytically. Their analysis demonstrates that a forbidden frequency gap for wave propagation along the y-direction (path OM) always exists. For $0 \leqslant p_B \leqslant 8/15$ the forbidden gap $(\sqrt{15}/2)\,p_B \leqslant \Omega \leqslant \sqrt{2}$ shrinks with increasing p_B. For $8/15 \leqslant p_B \leqslant 1$ the width of the forbidden gap $\sqrt{2} \leqslant \Omega \leqslant (\sqrt{15}/2)\,p_B$ grows. It stabilizes at $\sqrt{2} \leqslant \Omega \leqslant \sqrt{15}/2$ for $p_B \geqslant 1$. For waves propagating in the x-direction (path OK), the forbidden gap $3/2 \leqslant \Omega \leqslant \sqrt{15(1+3p_B)}/4$ opens for $p_B \geqslant 7/15$ and its width increases till $p_B = 1$. Combining the information about the mode frequencies in the critical points M, K and O, it can be predicted that a complete band gap opens above $\Omega = 3/2$ for $p_B > 3/5$. Its width grows up to a maximum value $3/2 \leqslant \Omega \leqslant \sqrt{15}/2$ when $p_B = 1$ and retains the same value on increasing p_B above 1. These theoretical predictions agree with the numerical results presented in figure 4.

For small values of the parameter p_B, the frequency of the lowest mode is proportional to the square root of p_B,

$$\Omega^2 \simeq 2p_B \sin^4 \beta/[1-(7/15)\sin^2 \beta], \tag{28}$$

demonstrating that propagation of this mode is due to the bending rigidity of the contacts. Measurements of the velocity of this mode provide direct access to the evaluation of bending rigidity.

Analytical expressions for some symmetry directions of propagation can be obtained. In particular, for waves propagating along the y-direction the rotation mode frequency is given by

$$\Omega_\Psi^2 = \tfrac{5}{4}\left[3+(p_B-1)\sin^2(\beta)\right], \tag{29}$$

and for waves propagating along the x-direction, the frequency of the rotation mode is

$$\Omega_\Phi^2 = \tfrac{15}{4}\left[1+(p_B-1)\sin^2(\alpha)\right]. \tag{30}$$

Dispersion curves for different bending parameter values are shown in figure 4 and verify the expressed analytical results. In figure 4 (and in the following), the color code (blue, green, red) corresponds to the order of appearance of the eigenvalues along the diagonal of the dynamical matrix **S** after a Schur decomposition. The Schur decomposition provides ordering of the eigenmodes (and consequently ordering of the associated eigenvalues) in accordance with the dominance of the component u, as a first criterion. If, for several modes, components u are equal, the ordering is obtained in accordance with the dominance of Φ, and finally, a comparison of the Ψ component is used if necessary. This ordering is used to attribute the successive colors blue, green and red to the three ordered eigenvalues in figure 4.

2.3. Normal contact with a rigid surface

We have analyzed the out-of-plane modes of a free suspended membrane considering both the rotational degrees of freedom of the particles and the finite size of the contact between beads. We include now the interaction with an infinitely rigid substrate supporting the membrane. The interaction with the substrate gives rise to the existence of additional forces and momenta at

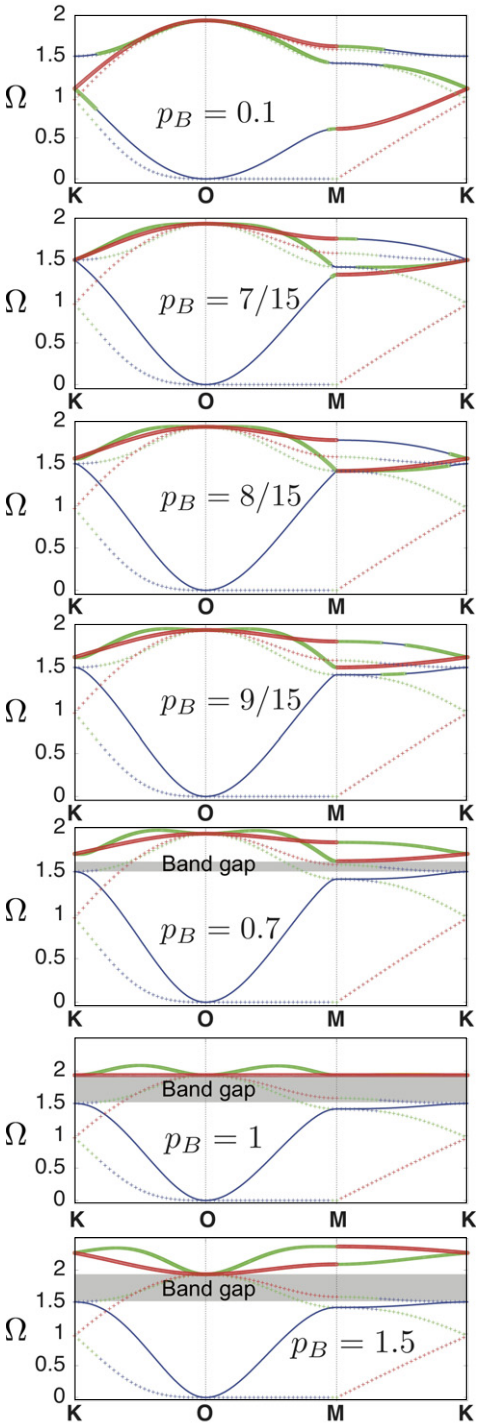

Figure 4. Dispersion curves obtained for different values of the parameter p_B of bending rigidity. The values of the bending parameter p_B are indicated and they increase from the top to the bottom panels. Dotted curves corresponding to the case of no bending rigidity, as in figure 2(a), are shown for comparison. The complete band gap is shown by the gray-shaded zone. The color code (blue, green, red) corresponds to the order of appearance of the eigenvalues along the diagonal of the dynamical matrix after a Schur decomposition.

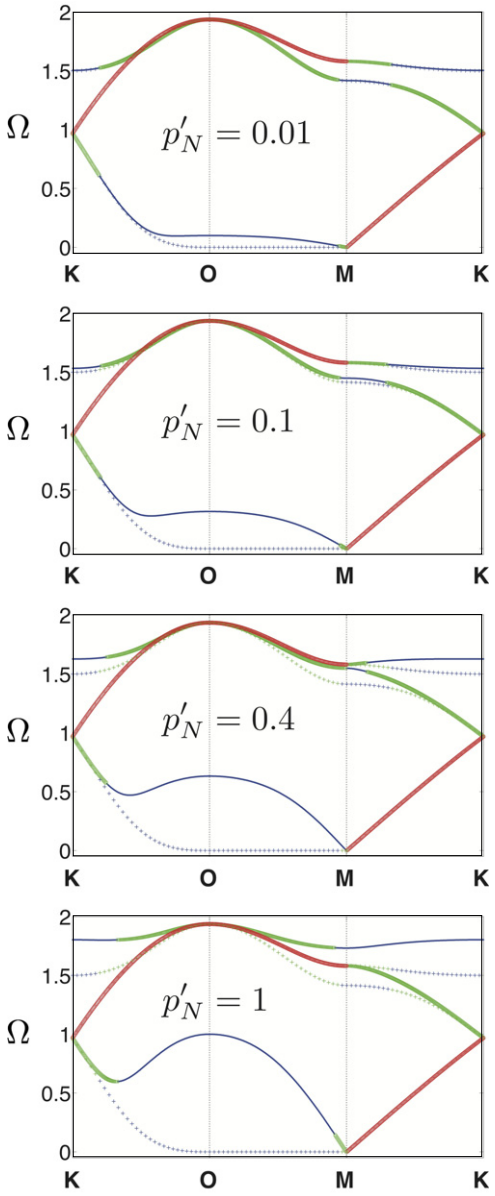

Figure 5. Dispersion curves obtained for different values of the parameter p'_{N} (normal rigidity between the beads and the substrate) and zero bending rigidity. Dotted curves corresponding to the case of no bending rigidity and no normal rigidity with the substrate, as in figure 2(a), are shown for comparison. The color code (blue, green, red) corresponds to the order of appearance of the eigenvalues along the diagonal of the dynamical matrix after a Schur decomposition.

the contact between an individual particle and the substrate, which are modeled as springs with their corresponding stiffness constant.

An additional returning force appears due to the motion along the z-axis, related to the normal rigidity of the contact of a sphere with the substrate ξ'_{N} (the symbol $'$ refers to the interaction with the rigid substrate).

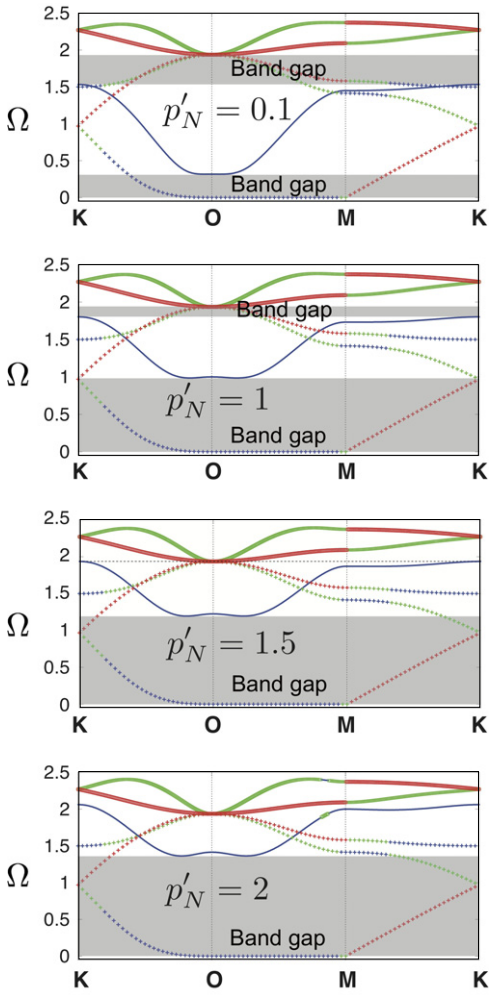

Figure 6. Dispersion curves obtained for different values of the parameter p'_{N} (normal rigidity between beads and the substrate) and for a fixed $p_{\mathrm{B}} = 1.5$ (bending rigidity between the beads). Dotted curves corresponding to the case of no bending rigidity and no normal rigidity with the substrate, as in figure 2(a), are shown for comparison. The color code (blue, green, red) corresponds to the order of appearance of the eigenvalues along the diagonal of the dynamical matrix after a Schur decomposition. The complete band gaps are shown by the gray-shaded zones.

This introduces modifications in only one term of S, given explicitly by

$$\Delta S'_{11} = -p'_{\mathrm{N}}, \tag{31}$$

where we have defined the adimensional parameter p'_{N} as $p'_{\mathrm{N}} = \xi'_{\mathrm{N}}/\xi$. The contact of the membrane with a rigid substrate has an influence on the dispersion relations.

The effect of normal rigidity in the absence of bending rigidity is shown in figure 5: when the membrane is on a rigid substrate it is composed rather of interacting oscillators than of oscillating masses. This manifests, in particular, in the fact that the wave with $\vec{k} = \vec{0}$, which corresponds to pure displacements without rotations, has now a non-zero frequency.

The growth of the frequency of the displacement-dominated lowest mode in the point O is described by $\Omega^2 = p'_N$ and is independent of the bending rigidity of the inter-bead contacts.

As follows from our analytical evaluations and figure 5 above, the displacement-dominated mode in the case $p'_N = 0$ becomes the lowest (in frequency) mode for $p_B \geqslant 7/15$ in the point K and for $p_B \geqslant 8/15$ in the point M. The analysis demonstrates that at larger values of p_B and non-zero values of p'_N the frequency of the lowest mode in these points depends only on the bead–substrate normal interactions: $\Omega^2 = (3/2)^2 + p'_N$ and $\Omega^2 = 2 + p'_N$ at the points K and M, respectively. Thus the continuous increase of p'_N for a fixed value of $p_B > 9/15$, where the complete band gap exists in the free-standing ($p'_N = 0$) membrane, will lead to closing of the complete gap. For $3/5 < p_B < 1$ the complete gap closes because the frequency of the first (lowest) mode at the point K becomes higher than the frequency of the second mode at the point M. This happens when $p'_N = \frac{3}{4}[5p_B - 3]$.

For $p_B \geqslant 1$ the complete band gap associated with bending rigidity (see figure 4) closes when p'_N becomes larger than $3/2$ because the frequency of the first (lowest) mode in the point K becomes higher than the coincident frequencies of the second and the third modes at the point O. In figure 6, we illustrate for $p_B = 1.5$ the closing of this complete gap, which is caused by the increased normal rigidity of the contacts between the beads constituting the membrane and the substrate. While this complete gap closes, the opening of a low-frequency complete band gap is also observed. This low-frequency complete band gap exists only if both bending rigidity of contacts between beads and normal rigidity of bead–substrate contacts are simultaneously non-zero. The bending rigidity is necessary to open a local low-frequency band gap at the point M, while the normal rigidity is necessary to open a local low-frequency band gap at the point O. For small values of the rigidities p_B and p'_N, these local gaps grow proportionally to corresponding rigidities (as $0 \leqslant \Omega \leqslant 15p_B/4$ and $0 \leqslant \Omega \leqslant p'_N$, respectively). Thus, for $p_r \ll 1$ and $p'_N \ll 1$, the complete low-frequency band gap is controlled by $\max(15p_B/4, p'_N)$ and experimental determination of the complete gap could provide a measure either of the bending rigidity of the contacts between the beads or of the normal rigidity of the bead–substrate contacts.

3. Conclusions

The above-presented results on the analytical and numerical evaluation of the out-of-plane motion of free-standing membranes composed of a single layer of ordered spherical particles demonstrate that, above a critical value of the ratio of bending to shear rigidity of the inter-particle contacts, a complete forbidden band gap for the elastic wave propagation exists. This complete band gap may disappear in the membranes supported by a substrate. Closing of the high-frequency ('optical') complete gap with increasing normal rigidity of the contacts between the particles and the rigid substrate has been predicted. Also, a low-frequency ('acoustical') complete band gap has been predicted to exist when the bending rigidity of contacts between beads and the normal rigidity of bead–substrate contacts are both important. More complex phenomena are expected if the shear rigidity of the contacts between the particles and the substrate is taken into consideration, because the shear rigidity of the particle–substrate contact couples the out-of-plane motion in the supported membranes to the in-plane motions. It would also be interesting to investigate in future the role of the spin (torsional) rigidity of the inter-particle contacts. The theoretical results presented above will guide the development of opto-acoustical methods for the non-destructive non-contact evaluation of the elastic properties

of free-standing and supported monolayer particle membranes [13–18, 20, 21], which are based on the all-optical monitoring of the elastic waves through both their generation and detection by lasers [50–52].

Acknowledgments

This work was supported by the STABINGRAM project (ANR-2010-BLAN-0927-03), by the MEC of the Spanish Government under project number FIS2008-06024-C03-03 and by the Jose Catillejo program. VT acknowledges the Universidad Politecnica de Valencia for support through a research visit fellowship.

Appendix

The elongation of the spring that models the contact is equal to the relative displacement δu_i of the 0 and i particles in this contact. This displacement is given by $\delta u_i = u_{0/i} - u_{i/i}$, where $u_{i/j}$ refers to the displacement of the i particle in the j contact. Explicitly, these displacement are given by

$$u_{0/1} = u_0 - \frac{\sqrt{3}}{2} R\varphi_0 - \frac{1}{2} R\psi_0, \qquad u_{1/1} = u_1 + \frac{\sqrt{3}}{2} R\varphi_1 + \frac{1}{2} R\psi_1,$$

$$u_{0/4} = u_0 + \frac{\sqrt{3}}{2} R\varphi_0 + \frac{1}{2} R\psi_0, \qquad u_{4/4} = u_4 - \frac{\sqrt{3}}{2} R\varphi_4 - \frac{1}{2} R\psi_4,$$

$$u_{0/3} = u_0 + \frac{\sqrt{3}}{2} R\varphi_0 - \frac{1}{2} R\psi_0, \qquad u_{3/3} = u_3 - \frac{\sqrt{3}}{2} R\varphi_3 + \frac{1}{2} R\psi_3,$$

$$u_{0/6} = u_0 - \frac{\sqrt{3}}{2} R\varphi_0 + \frac{1}{2} R\psi_0, \qquad u_{6/6} = u_6 + \frac{\sqrt{3}}{2} R\varphi_6 - \frac{1}{2} R\psi_6,$$

$$u_{0/2} = u_0 - R\psi_0, \qquad u_{2/2} = u_2 + R\psi_2,$$

$$u_{0/5} = u_0 + R\psi_0, \qquad u_{5/5} = u_5 - R\psi_5.$$

References

[1] Sheng P 2009 *Nat. Mater.* **8** 928
[2] Pennec Y *et al* 2010 *Surf. Sci. Rep.* **65** (8) 229
[3] Shelby R A, Smith D R and Schultz S 2001 *Science* **292** 77
[4] Sukhovich A *et al* 2009 *Phys. Rev. Lett.* **102** 154301
[5] Torrent D and Sanchez-Dehesa J 2008 *New J. Phys.* **10** 063015
[6] Zhang S, Yin L L and Fang N 2009 *Phys. Rev. Lett.* **102** 194301
[7] Mohammadi S *et al* 2007 *Electron. Lett.* **43** 898
[8] El Hassouani Y *et al* 2010 *Phys. Rev.* B **82** 7
[9] Yu D L *et al* 2006 *Phys. Lett.* A **357** 154
[10] Sadat-Saleh S *et al* 2009 *J. Appl. Phys.* **106** 074912
[11] Cheng Z, Russel W B and Chalkin P M 1999 *Nature* **401** 893
[12] Joannopoulos J D 2001 *Nature* **414** 257

[13] van Blaaden A, Ruel R and Wiltzius P 1997 *Nature* **385** 321
[14] Shevchenko E V, Talapin D V, O'Brien S and Murray C B 2005 *J. Am. Chem. Soc.* **127** 8741
[15] Shevchenko E V, Talapin D V, Murray C B and O'Brien S 2006 *J. Am. Chem. Soc.* **128** 3620
[16] Bigioni T P *et al* 2006 *Nat. Mater.* **5** 265
[17] Hossain M K 2007 *J. Lumin.* **122–123** 792
[18] Leahy B D *et al* 2010 *Phys. Rev. Lett.* **105** 058301
[19] Jiang C *et al* 2004 *Nat. Mater.* **3** 721
[20] Mueggenburg K E, Lin X-M, Goldsmith R H and Jaeger H M 2007 *Nat. Mater.* **6** 656
[21] Cheng W *et al* 2009 *Nat. Mater.* **8** 519
[22] Kittel C 2004 *Introduction to Solid State Physics* 8th edn (Berkeley, CA: Wiley and University of California) 2004
[23] Maradudin A A 1980 *Surface Phonons and Polaritons* (New York: Garland STPM Press)
[24] Blair D L, Mueggenburg N W, Marshall A H, Jaeger H M and Nagel S R 2001 *Phys. Rev.* E **63** 041304
[25] Nahmad-Molinari Y and Ruiz-Suarez J C 2002 *Phys. Rev. Lett.* **89** 264302
[26] Yu A B *et al* 2006 *Phys. Rev. Lett.* **97** 265501
[27] Carvente O and Ruiz-Suarez J C 2005 *Phys. Rev. Lett.* **95** 018001
[28] Schwartz L M, Johnson D L and Feng S 1984 *Phys. Rev. Lett.* **52** 831
[29] Bogdanov A N and Skvortsov A T 1992 *Sov. Phys. Acoust.* **38** 224
[30] Cosserat E and Cosserat F 1909 *Theorie Des Corps Deformables* (Paris: Herman et fils)
[31] Eringen A C 1999 *Microcontinuum Field Theories. 1: Foundations and Solids* (New York: Springer)
[32] Eringen A C 1968 Theory of micropolar elasticity *Fracture* ed H Liebowitz vol II (New York: Academic) chapter 7, pp 622–729
[33] Askar A and Cakmak A S 1968 *Int. J. Eng. Sci.* **6** 583
[34] Suiker A S J, Metrikine A V and de borst R 2001 *Int. J. Solids Struct.* **38** 1563
[35] Pavlov I S, Potapov A I and Maugin G A 2006 *Int. J. Solids Struct.* **43** 6194
[36] Kunin I A 1983 *Elastic Media with Microstructure Three-Dimensional Models* vol 2 (Berlin: Springer)
[37] Gassmann F 1951 *Geophysics* **16** 673
[38] Duffy J and Mindlin R D 1957 *J. Appl. Mech. Trans. ASME* **24** 585
[39] Stroll R D 1989 *Sediment Acoustics* (Berlin: Springer)
[40] White J E 1983 *Underground Sound* (Amsterdam: Elsevier)
[41] Inserra C, Tournat V and Gusev V E 2007 *Europhys. Lett.* **78** 44001
[42] Tournat V and Gusev V E 2010 *Acta Acust. United Acust.* **96** 208
[43] Gusev V E and Tournat V 2008 *Phys. Rev.* E **78** 036602
[44] Mouraille O, Mulder W A and Luding S 2006 *J. Stat. Mech.* (2006) P07023
[45] Merkel A, Tournat V and Gusev V E 2010 *Ultrasonics* **50** 133
[46] Merkel A, Tournat V and Gusev V E 2010 *Phys. Rev.* E **82** 031305
[47] Lyalin A E, Pirozhkov V A and Stepanov R D 1982 *Sov. Phys. Acoust.* **28** 494
[48] Kulesh M A, Matveenko V P and Shardakov I N 2005 *J. Appl. Mech. Tech. Phys.* **46** 556
[49] Johnson K L 1985 *Contact Mechanics* (Cambridge: Cambridge University Press)
[50] Thomsen C, Grahn H T, Maris H J and Tauc J 1986 *Phys. Rev.* B **34** 4129
[51] Scruby C B and Drain L E 1990 *Laser Ultrasonic Technique and Applications* (Bristol: Adam Hilger)
[52] Gusev V E and Karabutov A A 1993 *Laser Optoacoustics* (New York: AIP)